**www.lajss.org**
**Latin American Journal of Solids and Structures** 1 (2004) 379–399

# Characterization of bonded plates with Lamb and SH waves using a quasi-static approximation

Silvio de Barros[a,*], Antonio Lopes Gama[b], Martine Rousseau[c], Bernard Collet[c]

[a]Laboratoire d'Etudes Mécaniques des Assemblages - LEMA CNRS FRE 2481
Université de Versailles Saint-Quentin-en-Yvelines, Versailles, France
[b]Departamento de Engenharia Mecânica
Universidade Federal Fluminense, Niteroi, RJ, Brasil
[c]Laboratoire de Modélisation en Mécanique - LMM CNRS UMR 7607
Université Paris VI, Paris, France

Abstract

In this paper the propagation of guided Lamb waves and guided shear horizontally polarized (SH) waves in bonded plates is investigated. A model based on distributions of springs (quasi-static approximation) is used to describe the interaction of guided waves with imperfect adhesive layers. Through this approach, the imperfections of the adhesive layer were reproduced by changing the stiffness constant of the springs. The wave dispersion spectra for the Lamb waves and SH waves was obtained for different conditions of the adhesive layer. The influence of the adhesive mass on the dispersion curves of SH waves was also investigated. The results show that Lamb waves and the SH waves are sensitive to the alterations of the adhesive layer and have a great potential for the evaluation of bonded joints.

Keywords: Bonded joints, Lamb waves, SH waves, Spring-mass model

## 1 Introduction

The need for increasing structural performance, with low weight and high strength, has demanded the use of more effective joining methodologies. Mainly due to their low weight, low cost and ease of assembly, the adhesive bonds have emerged as a promising technology [9]. The widespread use of adhesive joints is also indicative of the advantages of the adhesive bonding over techniques such as welding and riveting. However, the use of adhesive bonding in aircraft structures and other safety critical applications has been limited due to the lack of adequate tools of design and control. Defects such as disbonds, voids and porosity; weak bond between the adhesive layer and adherent and a weak adhesive layer are commonly found in adhesive layers [8].

The development of numerical tools of design is necessary to increase the utilization of bonded joints in the industry. Interface damage models have been extensively used for the non-linear

* Corresp. author E-mail: silvio.debarros@meca.uvsq.fr Received 14 Sep 2004; In revised form 08 Dec 2004

incremental analysis of interface debonding in the last years [2–4, 6, 18]. This damage models used some parameters that can not be identified from mechanical tests. An acoustic procedure have been investigated for the evaluation of this interface parameters [28].

The great expansion of the use of bonded joints and bonded repairs has motivated the development of more reliable nondestructive methodologies. The conventional ultrasonic techniques, based on the echoes reflected by the defects, are not effective for inspection of most practical bonded joints due to the small thickness of the adhesive layer. In this case, the ultrasonic waves reflected by the interfaces of the adhesive layer are not separated in the time domain and interfere [14]. Also the conventional ultrasonic techniques are ineffective in interrogating large bonded areas. New methodologies using guided waves have been investigated for the inspection of bonded components. The primary advantage of using guided waves is that they can interrogate large areas, they also have many modes of propagation that can be selected according to the objective of the analysis [13, 17, 26].

In this paper, the propagation of guided Lamb waves and guided shear horizontally polarized waves (SH) in bonded plates is investigated. The quasi-static approximation (QSA) was used to describe the interaction of guided waves with imperfect adhesive layers. This model is based on the continuous distribution of springs to represent the adhesive layer. Through this approach, the imperfections of the adhesive layer can be reproduced by changing the stiffness constants of the springs [22, 27, 30]. The wave dispersion spectra for the Lamb waves and SH waves was obtained for different conditions of the adhesive layer. The results shown that ultrasonic guided waves have a great potential for the evaluation of bonded joints. The influence of the adhesive density on the dispersion curves of SH waves was also investigated. It is shown that the adhesive mass has little influence on the dispersion curves of SH waves.

## 2 The rheological interface model

Many articles are concerned with the study of the epoxy properties in a metal/epoxy/metal tri-layer model using leaky Lamb waves. Thus, Nagy and Adler [21], Jungman et al. [12], Lowe and Cawley [16], Kundu and Maslov [13] have experimentally revealed that the reflection and transmission coefficients are not very sensitive to the material properties. In order to model a thin adhesive layer, Jones and Whittier [11] introduced boundary conditions relating stresses and displacements with longitudinal and transversal stiffnesses. This model was then developed by Pilarski and Rose [23] and Rokhlin [25], while Rohklin and Wang [24] introduced a viscoelastic rheological model (complex springs stiffnesses).

The rheological model allows the identification of adhesion parameters, while the tri-layer model is more appropriated to study the cohesive properties. A good condition of adhesion can be identified by comparing acoustic tests results and the theorical results obtained by the rheological model [29].

The adhesive joint consists of two elastic bodies (adherends) joined by a plane adhesive layer

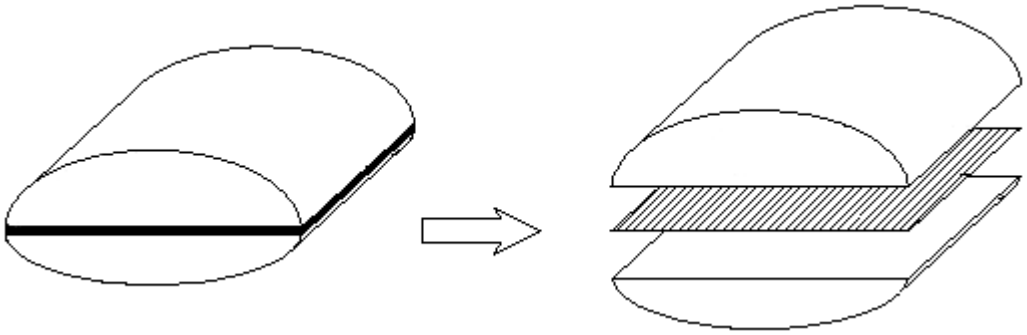

Figure 1: Bonded interface.

the thickness of which is assumed to be negligible compared to both that of the joined bodies and to its in-plane dimensions. These features enable the adhesive layer to be conveniently schematized as an interface, i.e. as a zero-thickness surface entity which ensures displacement and stress transfer between the adherends, as depicted in Figure 1.

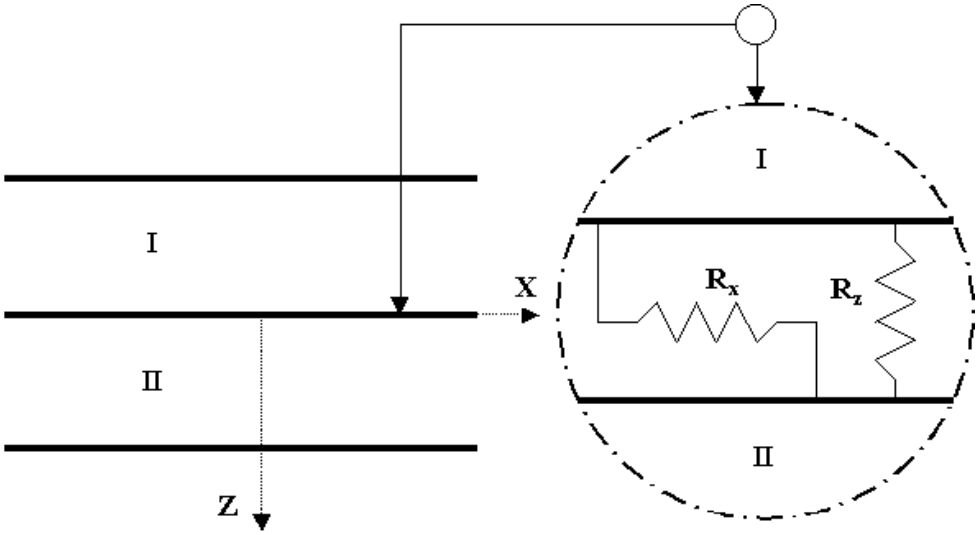


Figure 2: Model of the adhesive layer.

Interface damage models consider the damage $d$ as a variable that changes the stiffnesses of an elastic interface, as shown in Figure 2. In equation 1 the interface stiffnesses $R_i$ are calculated as a function of their initial value $R_i^0$ and a damage value, with $0 \leq d \leq 1$. When $d = 0$ the interface is simply elastic without damage and when $d$ reach the value 1 the interface is completely debonded.

$$R_i = R_i^0 (1 - d) \Rightarrow i = x, y, z \tag{1}$$

The stiffnesses of a thin layer of adhesive can not be easily derived from the elastic properties of the adhesive itself. They can not be identified from mechanical tests on adhesively bonded assemblies as they have a small influence on the global response of the assembly, but they can be identified from acoustical tests.

## 3 Propagation of Lamb waves and SH waves in a homogeneous infinite plate

The basic concepts of wave propagation will be introduced through the analysis of Lamb waves propagation in a homogeneous infinite plate, Figure 3 [1,7]. We consider a plane strain state in the xz plane and consequently the propagation of longitudinal (P) and transverse (SV) waves. We define the wave numbers: $k_L = \omega/c_L$ and $k_T = \omega/c_T$ , where $c_L$ and $c_T$ are the longitudinal and transverse wave speed respectively and $\omega$ is the angular frequency.

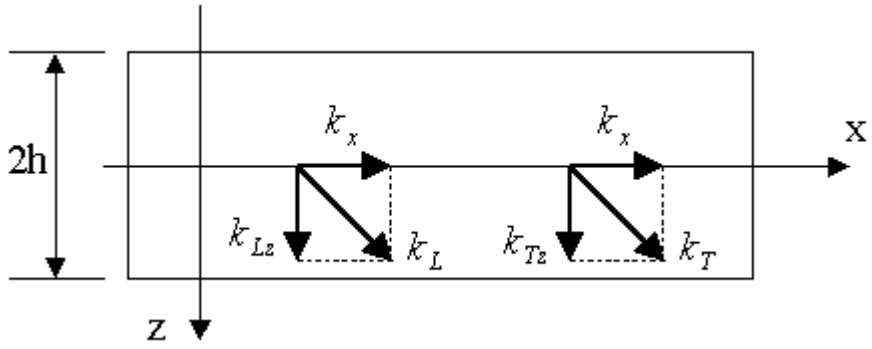


Figure 3: Infinite plate of thickness 2h.

For a homogeneous isotropic plate, the Naviers equation can be written:

$$\mu \nabla^2 \mathbf{u} + (\lambda + \mu) \nabla \nabla \cdot \mathbf{u} = \rho \ddot{\mathbf{u}} \tag{2}$$

where $\lambda$ and $\mu$ are the Lamé's coefficients. Using the Helmholtz's decomposition, we can write the displacements in the following form:

$$\mathbf{u} = \nabla \varphi + \nabla \wedge \psi \tag{3}$$

where $\varphi$ is a scalar potential and $\psi$ is a vector potential, with the constraint condition $\nabla \cdot \psi = 0$.

For a time-harmonic wave motion and grouping the symmetric and anti-symmetric components, the scalar and vector potentials can be expressed as:

$$\begin{array}{c} \varphi = \left[S_L \cos\left(k_{Lz} z\right) + A_L \sin\left(k_{Lz} z\right)\right] e^{i(k_x x - \omega t)} \\ \psi_y = \left[A_T \cos\left(k_{Tz} z\right) + S_T \sin\left(k_{Tz} z\right)\right] e^{i(k_x x - \omega t)} \\ \psi_x = \psi_z = 0 \end{array} \tag{4}$$

Where $k_x$, $k_{Lz}$ and $k_{Tz}$ are shown in Figure 3 ( $k_L^2 = k_x^2 + k_{Lz}^2$ and $k_T^2 = k_x^2 + k_{Tz}^2$ ). $S$ and $A$ represent the symmetric and anti-symmetric components. $L$ and $T$ refer to the components of longitudinal and transverse waves respectively. The components of the displacement vector $\mathbf{u}$ can be determined substituting Eq. 4 in Eq. 3:

$$\begin{array}{rcc} u_x & = & \left[ik_x S_L \cos\left(k_{Lz} z\right) + ik_x A_L \sin\left(k_{Lz} z\right) + \right. \\ & & \left. + k_{Tz} A_T \sin\left(k_{Tz} z\right) - k_{Tz} S_T \cos\left(k_{Tz} z\right)\right] e^{i(k_x x - \omega t)} \\ u_z & = & \left[-k_{Lz} S_L \sin\left(k_{Lz} z\right) + k_{Lz} A_L \cos\left(k_{Lz} z\right) + \right. \\ & & \left. + ik_x A_T \cos\left(k_{Tz} z\right) + ik_x S_T \sin\left(k_{Tz} z\right)\right] e^{i(k_x x - \omega t)} \end{array} \tag{5}$$

Using the Hooke's law, the stress components can be given by:

$$\begin{array}{rcc} \sigma_{xz} & = & \mu\left[-2ik_{Lz}k_x S_L \sin\left(k_{Lz} z\right) + S_T\left(k_T^2 - 2k_x^2\right) \sin\left(k_{Tz} z\right) + \right. \\ & & \left. + 2ik_{Lz}k_x A_L \cos\left(k_{Lz} z\right) + A_T\left(k_T^2 - 2k_x^2\right) \cos\left(k_{Tz} z\right)\right] e^{i(k_x x - \omega t)} \\ \sigma_{zz} & = & \mu\left[-S_L\left(k_T^2 - 2k_x^2\right) \cos\left(k_{Lz} z\right) + 2ik_{Tz}k_x S_T \cos\left(k_{Tz} z\right) + \right. \\ & & \left. - A_L\left(k_T^2 - 2k_x^2\right) \sin\left(k_{Lz} z\right) - 2ik_{Tz}k_x A_T \sin\left(k_{Tz} z\right)\right] e^{i(k_x x - \omega t)} \end{array} \tag{6}$$

The boundary conditions for the free surfaces of the plate are:

$$\begin{array}{rcl} \sigma_{xz} = 0 & \Rightarrow & z = \pm h \forall x, t \\ \sigma_{zz} = 0 & \Rightarrow & z = \pm h \forall x, t \end{array} \tag{7}$$

Applying the boundary conditions in Eq. 6, we can find a system of equations that will be decomposed in two systems: one for the symmetric and the other for the anti-symmetric modes.

For the symmetric modes we obtain:

$$\begin{bmatrix} -2ik_{Lz}k_x \sin\left(k_{Lz} h\right) & \left(k_T^2 - 2k_x^2\right) \sin\left(k_{Tz} h\right) \\ -\left(k_T^2 - 2k_x^2\right) \cos\left(k_{Lz} h\right) & 2ik_{Tz}k_x \cos\left(k_{Tz} h\right) \end{bmatrix} \begin{Bmatrix} S_L \\ S_T \end{Bmatrix} = \begin{Bmatrix} 0 \\ 0 \end{Bmatrix} \tag{8}$$

and for the anti-symmetric modes:

$$\begin{bmatrix} 2ik_{Lz}k_x \cos\left(k_{Lz} h\right) & \left(k_T^2 - 2k_x^2\right) \cos\left(k_{Tz} h\right) \\ \left(k_T^2 - 2k_x^2\right) \sin\left(k_{Lz} h\right) & 2ik_{Tz}k_x \sin\left(k_{Tz} h\right) \end{bmatrix} \begin{Bmatrix} A_L \\ A_T \end{Bmatrix} = \begin{Bmatrix} 0 \\ 0 \end{Bmatrix} \tag{9}$$

The phase velocities for an aluminium plate are shown in Figure 4. The modulus of elasticity and Poisson's ratio for aluminium are the same for all plots in this paper: $E = 71 \times 10^9 MPa$ and $\nu = 0.3$. The branches shown in Figure 4 correspond to the non-trivial solutions of Eq.8 and Eq.9. The solutions are given for vanishing determinate and they were calculated numerically using a routine implemented with the aid of the commercial code MATLAB$^{TM}$.

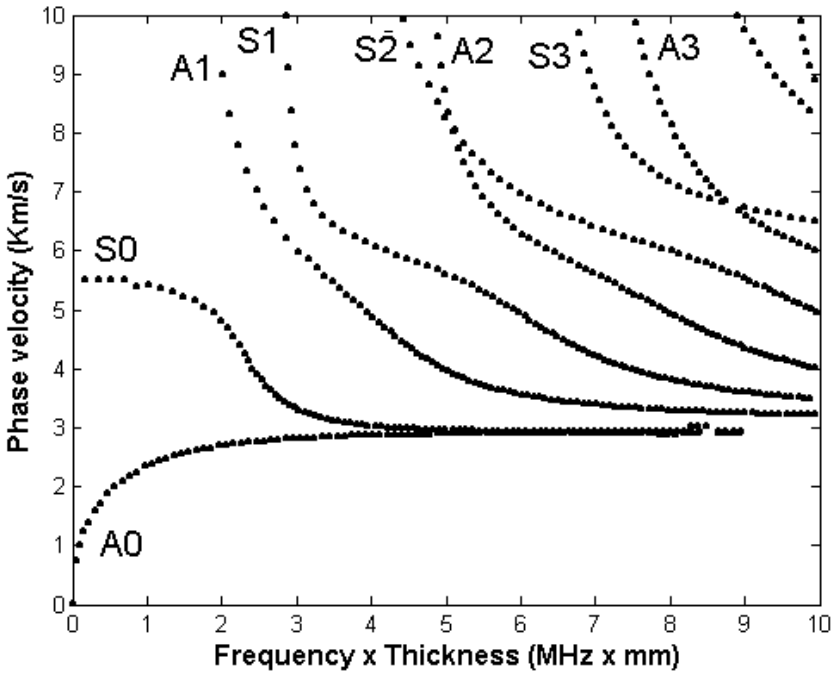


Figure 4: Dispersion curves for Lamb waves in an aluminium plate.

The SH waves have displacement components in the $y$ direction only. For a time-harmonic wave motion the displacement in the $y$ direction can be written in the form:

$$u_y = \left[B_1 \cos\left(k_{Tz} z\right) + B_2 \sin\left(k_{Tz} z\right)\right] e^{i(k_x x - \omega t)} \tag{10}$$

Due to the lack of space the details to obtain the frequency equation for SH waves will be omitted here. The complete procedure can be found in [1]. The dispersion curves for the SH-modes in an aluminium plate is shown in Figure 5 .

## 4 Propagation of Lamb waves in bonded plates

In this section a model based on the continuous distribution of springs is used to describe the adhesive layer as shown in Figure 2. This procedure is known as the quasi-static approximation (QSA) [5]. Through this approach the defects of the adhesive layer can be simulated changing the stiffness constants of the springs [22, 27, 30].

The objective of this section is to investigate the propagation of Lamb waves in two bonded plates for different conditions of the adhesive layer.

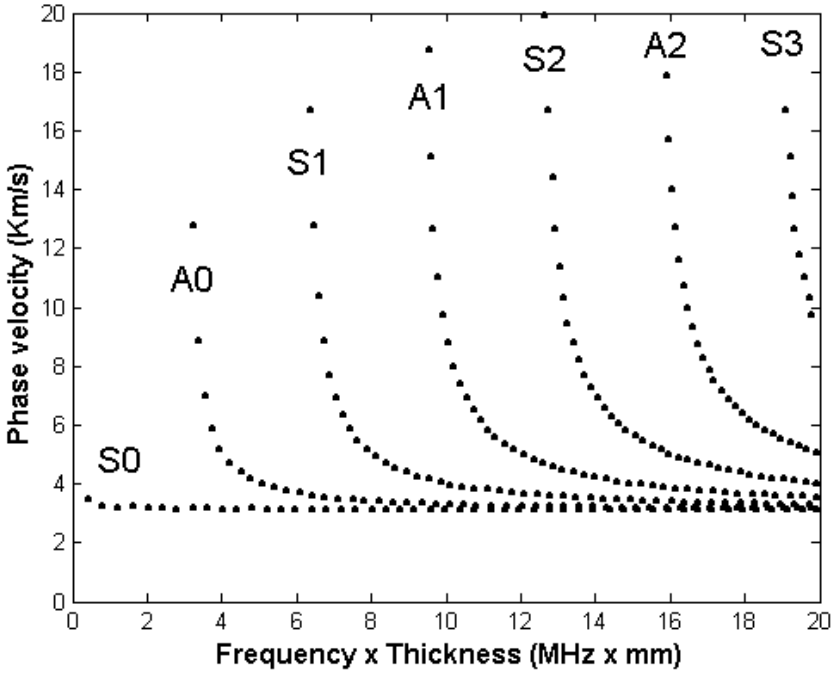


Figure 5: Dispersion curves for SH waves in an aluminium plate.

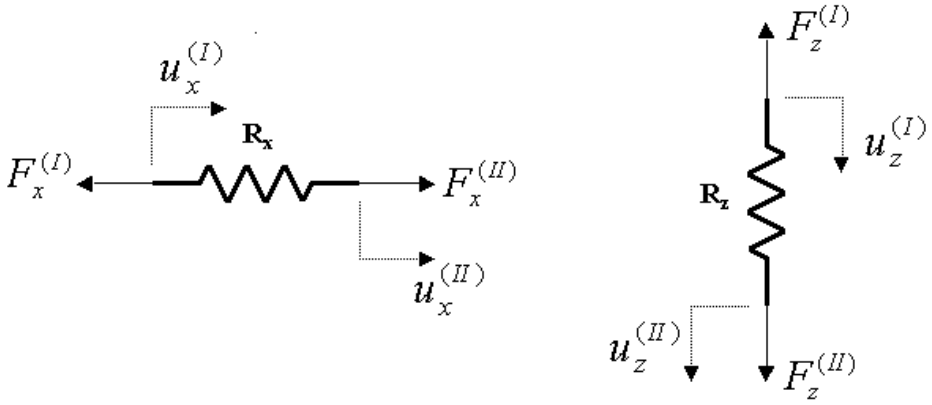


Figure 6: Forces and displacements on the springs.

In this model the plates $(I)$ and $(II)$, shown in Figure 2, may have diferent thicknesses $h_1$ and $h_2$ but the results presented hereafter consider $h_1 = h_2 = h$. In the following equations the superscripts $(I)$ and $(II)$ are used for referring to plate $(I)$ and plate $(II)$ respectively, as shown in Figure 6.

Applying the boundary conditions in Eqs. 6, for the free surface of plate I and plate II, we obtain the following equations:

$$\sigma_{xz}^{(I)} = 0 \quad \Rightarrow \quad z = -h_1 \,\forall\, x, t$$

$$\begin{gathered} 2ik_{Lz}k_x \sin\left(k_{Lz}h_1\right) S_L^{(I)} - \left(k_T^2 - 2k_x^2\right) \sin\left(k_{Tz}h_1\right) S_T^{(I)} + \\ +2ik_{Lz}k_x \cos\left(k_{Lz}h_1\right) A_L^{(I)} + \left(k_T^2 - 2k_x^2\right) \cos\left(k_{Tz}h_1\right) A_T^{(I)} = 0 \end{gathered} \tag{11}$$

$$\sigma_{zz}^{(I)} = 0 \quad \Rightarrow \quad z = -h_1 \,\forall\, x, t$$

$$\begin{gathered} -\left(k_T^2 - 2k_x^2\right) \cos\left(k_{Lz}h_1\right) S_L^{(I)} + 2ik_{Tz}k_x \cos\left(k_{Tz}h_1\right) S_T^{(I)} + \\ +\left(k_T^2 - 2k_x^2\right) \sin\left(k_{Lz}h_1\right) A_L^{(I)} + 2ik_{Tz}k_x \sin\left(k_{Tz}h_1\right) A_T^{(I)} = 0 \end{gathered} \tag{12}$$

$$\sigma_{xz}^{(II)} = 0 \quad \Rightarrow \quad z = h_2 \,\forall\, x, t$$

$$\begin{gathered} -2ik_{Lz}k_x \sin\left(k_{Lz}h_2\right) S_L^{(II)} + \left(k_T^2 - 2k_x^2\right) \sin\left(k_{Tz}h_2\right) S_T^{(II)} + \\ +2ik_{Lz}k_x \cos\left(k_{Lz}h_2\right) A_L^{(II)} + \left(k_T^2 - 2k_x^2\right) \cos\left(k_{Tz}h_2\right) A_T^{(II)} = 0 \end{gathered} \tag{13}$$

$$\sigma_{zz}^{(II)} = 0 \quad \Rightarrow \quad z = h_2 \,\forall\, x, t$$

$$\begin{gathered} -\left(k_T^2 - 2k_x^2\right) \cos\left(k_{Lz}h_2\right) S_L^{(II)} + 2ik_{Tz}k_x \cos\left(k_{Tz}h_2\right) S_T^{(II)} + \\ -\left(k_T^2 - 2k_x^2\right) \sin\left(k_{Lz}h_2\right) A_L^{(II)} - 2ik_{Tz}k_x \sin\left(k_{Tz}h_2\right) A_T^{(II)} = 0 \end{gathered} \tag{14}$$

For $z = 0$ the boundary conditions in the adhesive layer can be written as:

$$\sigma_{xz}^{(I)} = \widehat{R}_x \left(u_x^{(II)} - u_x^{(I)}\right) \tag{15}$$

$$\sigma_{zz}^{(I)} = \widehat{R}_z \left(u_z^{(II)} - u_z^{(I)}\right) \tag{16}$$

$$\sigma_{xz}^{(II)} = \sigma_{xz}^{(I)} \tag{17}$$

$$\sigma_{zz}^{(II)} = \sigma_{zz}^{(I)} \tag{18}$$

where $\widehat{R}_x = \frac{R_x}{S}$ and $\widehat{R}_z = \frac{R_z}{S}$ . $S$ is the interface area.

Using the Eqs. 5 and 6 for $z = 0$, the expressions for the displacements and stresses on the interfaces can be given by:

$$u_x^{(I)} = \left[ iS_L^{(I)} k_x - S_T^{(I)} k_{Tz} \right] e^{i(k_x x - \omega t)} \tag{19}$$

$$u_z^{(I)} = \left[ A_L^{(I)} k_{Lz} + iA_T^{(I)} k_x \right] e^{i(k_x x - \omega t)} \tag{20}$$

$$u_x^{(II)} = \left[ iS_L^{(II)} k_x - S_T^{(II)} k_{Tz} \right] e^{i(k_x x - \omega t)} \tag{21}$$

$$u_z^{(II)} = \left[ A_L^{(II)} k_{Lz} + iA_T^{(II)} k_x \right] e^{i(k_x x - \omega t)} \tag{22}$$

$$\sigma_{xz}^{(I)} = \mu \left[ 2iA_L^{(I)} k_{Lz} k_x + A_T^{(I)} \left( k_T^2 - 2k_x^2 \right) \right] e^{i(k_x x - \omega t)} \tag{23}$$

$$\sigma_{zz}^{(I)} = \mu \left[ 2iS_T^{(I)} k_{Tz} k_x - S_L^{(I)} \left( k_T^2 - 2k_x^2 \right) \right] e^{i(k_x x - \omega t)} \tag{24}$$

$$\sigma_{xz}^{(II)} = \mu \left[ 2iA_L^{(II)} k_{Lz} k_x + A_T^{(II)} \left( k_T^2 - 2k_x^2 \right) \right] e^{i(k_x x - \omega t)} \tag{25}$$

$$\sigma_{zz}^{(II)} = \mu \left[ 2iS_T^{(II)} k_{Tz} k_x - S_L^{(II)} \left( k_T^2 - 2k_x^2 \right) \right] e^{i(k_x x - \omega t)} \tag{26}$$

By applying Eqs. 19 to 26 in Eqs. 15 to 18 we obtain the following equations:

$$\begin{gathered} ik_x S_L^{(I)} - k_{Tz} S_T^{(I)} - ik_x S_L^{(II)} + k_{Tz} S_T^{(II)} + \\ + \tfrac{\mu}{\widehat{R}_x} 2ik_{Lz} k_x A_L^{(II)} + \tfrac{\mu}{\widehat{R}_x} \left( k_T^2 - 2k_x^2 \right) A_T^{(II)} = 0 \end{gathered} \tag{27}$$

$$\begin{gathered} k_{Lz} A_L^{(I)} + ik_x A_T^{(I)} - \tfrac{\mu}{\widehat{R}_z} \left( k_T^2 - 2k_x^2 \right) S_L^{(II)} + \\ + \tfrac{\mu}{\widehat{R}_z} 2ik_{Tz} k_x S_T^{(II)} - k_{Lz} A_L^{(II)} - ik_x A_T^{(II)} = 0 \end{gathered} \tag{28}$$

$$2ik_{Lz} k_x A_L^{(I)} + \left( k_T^2 - 2k_x^2 \right) A_T^{(I)} - 2ik_{Lz} k_x A_L^{(II)} - \left( k_T^2 - 2k_x^2 \right) A_T^{(II)} = 0 \tag{29}$$

$$- \left( k_T^2 - 2k_x^2 \right) S_L^{(I)} + 2ik_{Tz} k_x S_T^{(I)} + \left( k_T^2 - 2k_x^2 \right) S_L^{(II)} + 2ik_{Tz} k_x S_T^{(II)} = 0 \tag{30}$$

The solutions of the system of Eqs. 11 to 14 and Eqs. 27 to 30 constitutes the dispersion curves for the Lamb waves in the two bonded plates. The solutions are given for vanishing determinate and they were calculated numerically using a routine implemented with the aid of the commercial code MATLAB$^{TM}$.

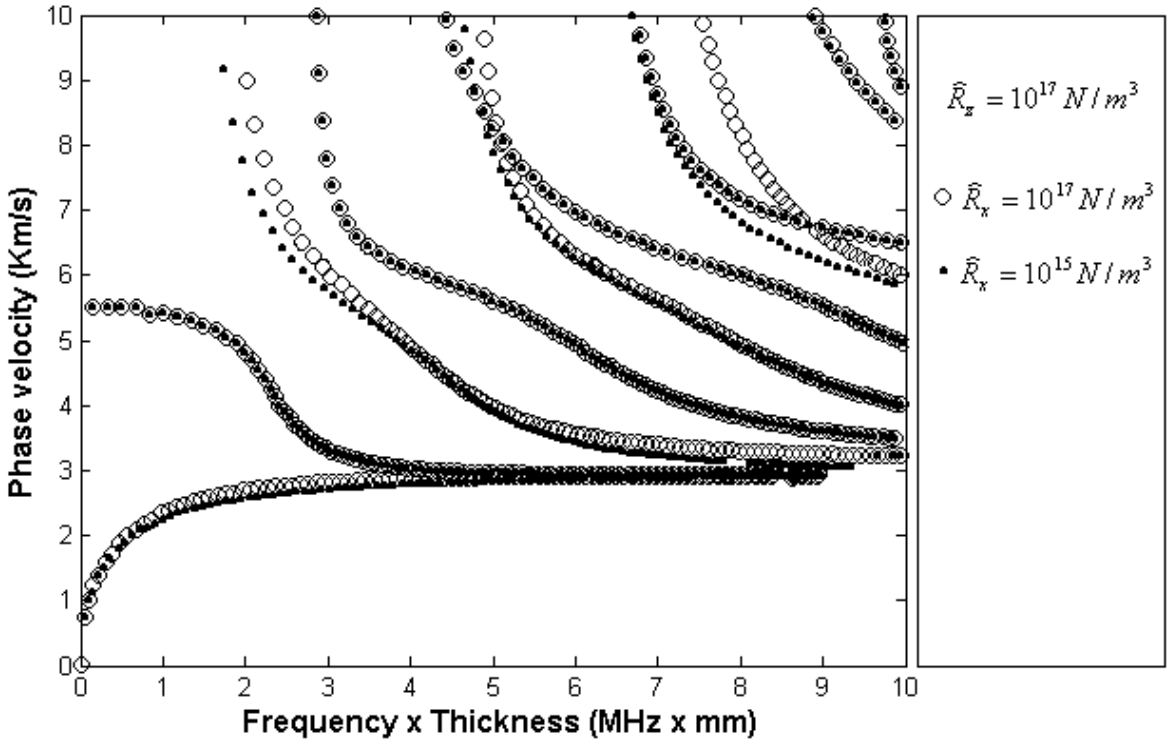


Figure 7: Dispersion curves.

### 4.1 Dispersion curves of Lamb waves in bonded plates

The dispersion curves of Lamb waves was obtained for different conditions of the adhesive layer. First the perfect adhesion was simulated by assuming very high values for $\widehat{R}_x$ and $\widehat{R}_z$. In this case the stiffness of the adhesive layer is considered infinite. For this condition, the dispersion curves for the aluminium bonded plates was compared with the dispersion curves for a single aluminium plate of thickness 2h and the results shown an excellent agreement. We concluded that the stiffness of $1 \times 10^{17} N/m^3$ for $\widehat{R}_x$ and $\widehat{R}_z$ can represent the case of a perfect adhesion for the two bonded aluminium plates. Next, the stiffness of the springs was gradually reduced to simulate deficient conditions of the adhesive layer. Figures 7 and 8 show the dispersion curves for $\widehat{R}_x = 10^{15} N/m^3$ and $\widehat{R}_z = 10^{17} N/m^3$, and the dispersion curves for $\widehat{R}_x = 10^{17} N/m^3$ and $\widehat{R}_z = 10^{15} N/m^3$, respectively. For both cases the results are compared with the ideal condition of adhesion ($\widehat{R}_x = \widehat{R}_z = 10^{17} N/m^3$).

The dispersion curves of Figures 7 and 8 show that only the anti-symmetric modes change when reducing $\widehat{R}_x$ and only the symmetric modes change when reducing $\widehat{R}_z$ . This can also be concluded regarding Eq. 5 for $z = 0$, where for the symmetric modes, the symmetric part of $u_x$

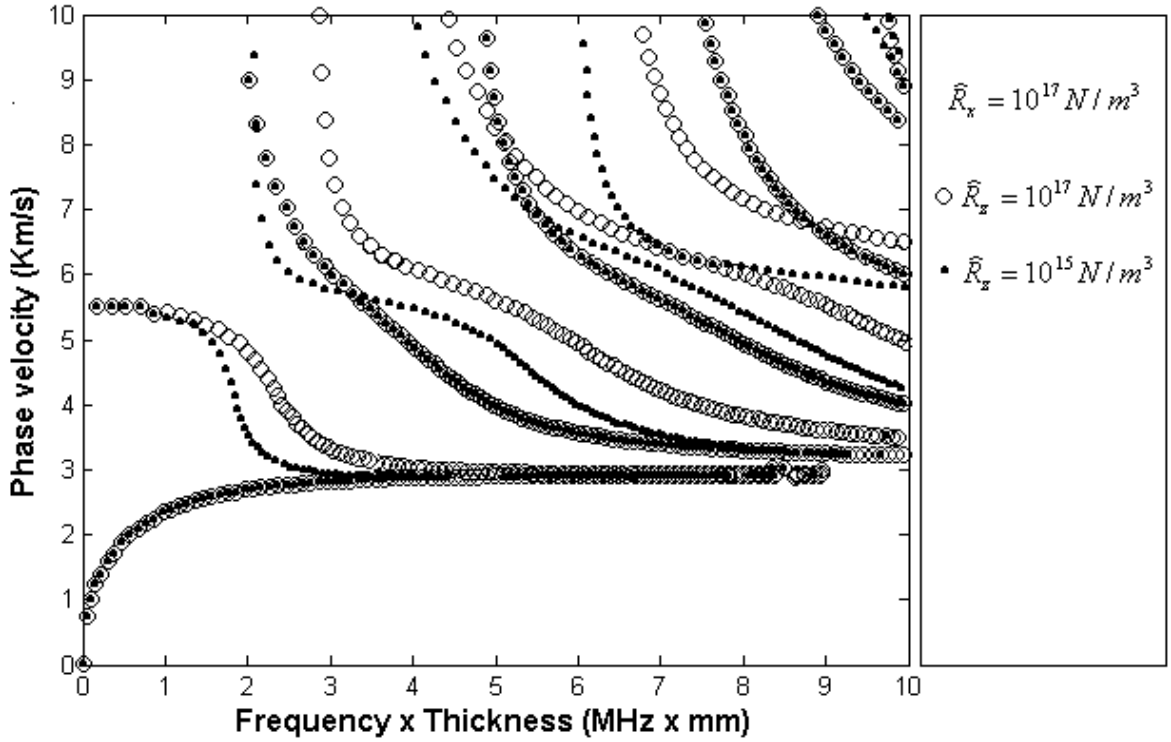


Figure 8: Dispersion curves.

is zero and for the anti-symmetric modes, the anti-symmetric part of $u_z$ is zero.

The phase velocity in function of $\widehat{R}_x$ for the first anti-symmetric mode A0 is shown in detail in Figure 9, while the Figure 10 shows the phase velocity for the first symmetric mode S0 in function of $\widehat{R}_z$ . Accordingly with Figures 9 and 10, the phase velocity for both modes decrease due to the reduction of the stiffness of the adhesive layer.

We observed that the Lamb wave modes are sensitive to the alterations of the adhesive layer and that the general condition of the adhesive layer can be described by monitoring the propagation of Lamb waves. Recent ultrasonic techniques using guided waves are able to excite only some Lamb wave modes [19]. Also, as reported by [9] and [20], variations of the phase velocity of Lamb waves can be used to evaluate the conditions of the adhesive layer.

## 5 Propagation of SH waves in bonded plates

In this section, the quasi-static approximation is also used to simulate the propagation of SH waves in aluminium bonded plates, as shown in Figures 11 and 12. The SH waves have dis-

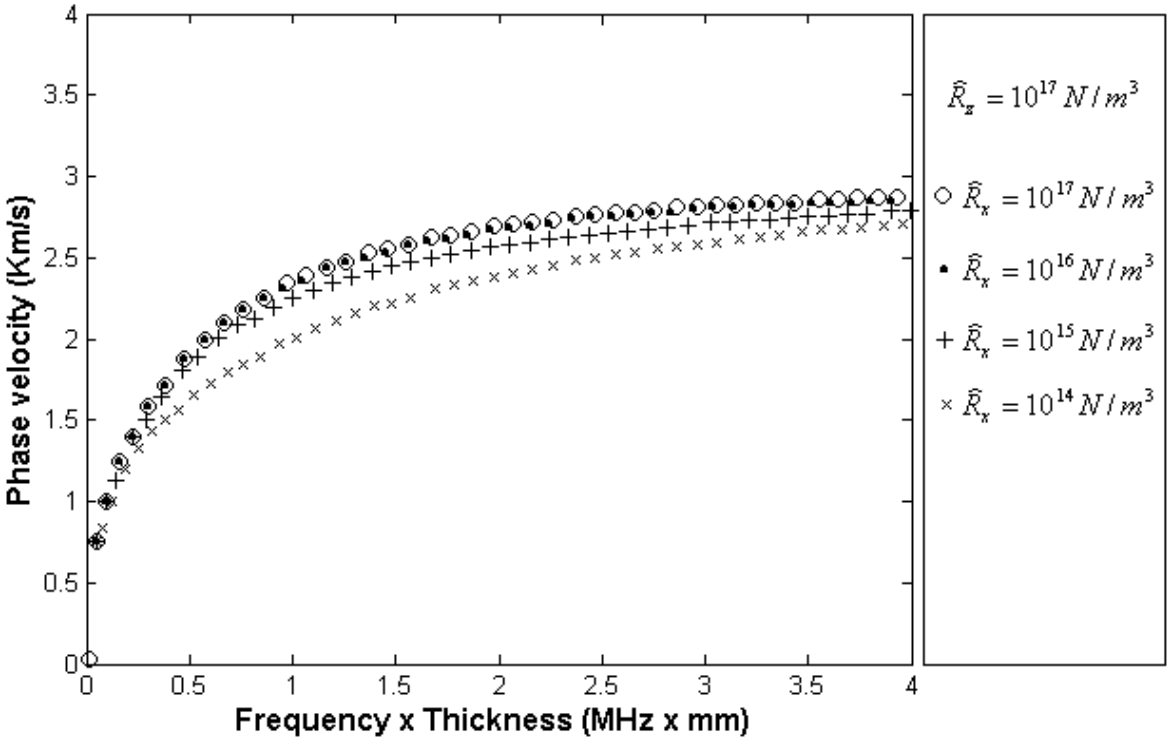


Figure 9: Dispersion curves for A0.

placement components in the $y$ direction and consequently, only the springs in the $y$ direction are considered. Although the SH waves are difficult to excite, some techniques using guided SH waves for nondestructive evaluation have been reported [10, 31].

As for the case of a single plate [1], the displacement $u_y$ for each plate can be given by:

$$\begin{cases} u_y^{(I)} &= \left[B_1 \cos\left(k_{Tz} z\right) + B_2 \sin\left(k_{Tz} z\right)\right] e^{i(k_x x - \omega t)} \\ u_y^{(II)} &= \left[B_3 \cos\left(k_{Tz} z\right) + B_4 \sin\left(k_{Tz} z\right)\right] e^{i(k_x x - \omega t)} \end{cases} \tag{31}$$

Using the Hookes' law, we can find that :

$$\sigma_{yz} = \mu u_y \tag{32}$$

Applying the boundary conditions $\sigma_{xz} = \sigma_{yz} = \sigma_{zz} = 0$ , for the free surfaces $z = h_1$ and $z = -h_2$ :

$$\begin{cases} u_y^{(I)} &= 0 \\ u_y^{(II)} &= 0 \end{cases} \tag{33}$$

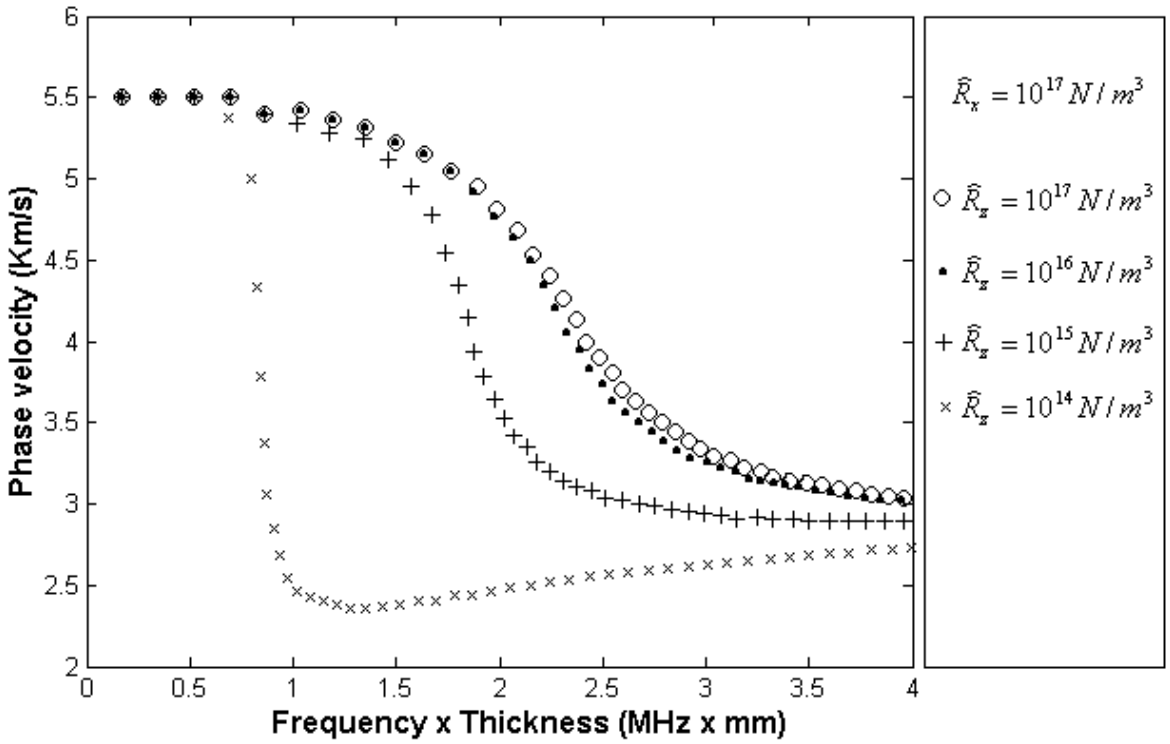


Figure 10: Dispersion curves for S0.

Next, applying the conditions given by Eq. 33 in Eq. 31, we can find the following equations:

$$\begin{cases} -B_1 \sin(k_{Tz} h_1) + B_2 \cos(k_{Tz} h_1) &= 0 \\ B_3 \sin(k_{Tz} h_2) + B_4 \cos(k_{Tz} h_2) &= 0 \end{cases} \tag{34}$$

For $z = 0$ the boundary conditions in the adhesive layer can be written as:

$$\sigma_{yz}^{(I)} = -\widehat{R}_y \left( u_y^{(II)} - u_y^{(I)} \right) \tag{35}$$

$$\sigma_{yz}^{(I)} = \sigma_{yz}^{(II)} \Rightarrow \mu u_y^{(I)} - \mu u_y^{(II)} \Rightarrow u_y^{(I)} = u_y^{(II)} \tag{36}$$

where $\widehat{R}_y = \frac{R_y}{S}$.
Applying Eq. 36 in Eqs. 31 for $z = 0$, we find that:

$$B_2 - B_4 = 0 \tag{37}$$

Using Eq. 32, Eq. 35, and Eq. 31, we obtain:

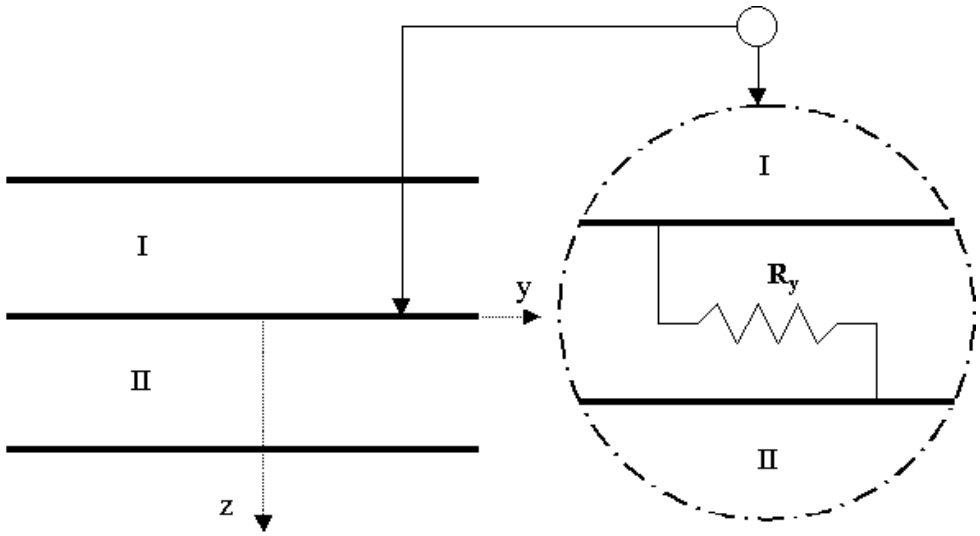


Figure 11: Interface model.

$$-\widehat{R}_y B_1 + \mu k_{Tz} B_2 + \widehat{R}_y B_3 = 0 \tag{38}$$

Equations 34, 37 and 38 may be rewritten in matrix form:

$$\begin{bmatrix} -\sin(k_{Tz}h_1) & \cos(k_{Tz}h_1) & 0 & 0 \\ 0 & 0 & \sin(k_{Tz}h_2) & \cos(k_{Tz}h_2) \\ -\widehat{R}_y & \mu k_{Tz} & \widehat{R}_y & 0 \\ 0 & 1 & 0 & -1 \end{bmatrix} \begin{Bmatrix} B_1 \\ B_2 \\ B_3 \\ B_4 \end{Bmatrix} = 0 \tag{39}$$

The solutions of the system of Eqs. 39 constitutes the dispersion curves for the SH waves for the two bonded plates. The solutions are given for vanishing determinate and they were calculated numerically using a routine implemented with the aid of the commercial code MATLAB$^{TM}$.

### 5.1 SH waves in bonded plates

The same procedure used to investigate the propagation of Lamb waves in bonded plates, as described in section 3, was applied here to study the propagation of SH waves. The dispersion curves of SH waves was also obtained for different conditions of the adhesive layer, using Eq. 39, beginning with the perfect adhesion ($\widehat{R}_y = 10^{17} N/m^3$) and gradually decreasing the stiffness of the spring to simulate deficient conditions of the adhesive layer. Figure 13 shows the dispersion curves of SH waves for different stiffness constant $\widehat{R}_y$. Note that only the branches of the anti-symmetric modes change and become closer to the branches of the symmetric modes for low $\widehat{R}_y$.

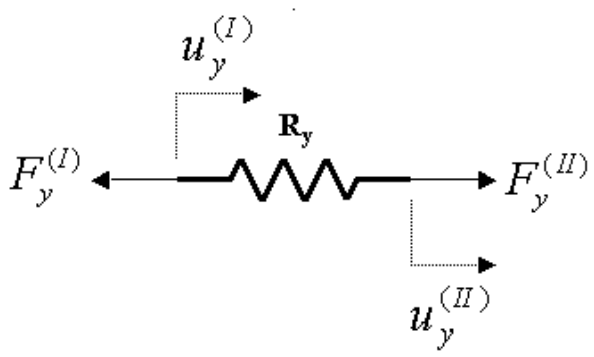


Figure 12: Forces and displacements on the springs.

Figure 14 show the phase velocity curves for the first anti-symmetric mode A0 for different stiffness constant $\widehat{R}_y$.

### 5.2 The spring-mass model

The SH waves were also employed to study the influence of the adhesive mass [15]. In this case, a model based on the continuous distribution of springs and masses is used to describe the adhesive layer as shown in Figures 15 and 16.

The following procedure is described in order to obtain the dispersion curves of SH waves using the model shown in Figures 15 and 16. The same boundary conditions $\sigma_{xz} = \sigma_{yz} = \sigma_{zz} = 0$, are considered for the free surfaces $z = h_1$ and $z = -h_2$. For the interface we can write:

$$\sigma_{yz}^{(I)} = -\widehat{R}_y \left( u_y^{(m)} - u_y^{(I)} \right) \Rightarrow u_{y,z}^{(I)} = \frac{\widehat{R}_y}{\mu} \left( u_y^{(I)} - u_y^{(m)} \right) \tag{40}$$

$$\sigma_{yz}^{(II)} = \widehat{R}_y \left( u_y^{(m)} - u_y^{(II)} \right) \Rightarrow u_{y,z}^{(II)} = \frac{\widehat{R}_y}{\mu} \left( u_y^{(m)} - u_y^{(II)} \right) \tag{41}$$

From Eq. 31, Eq. 40 and Eq. 41, we obtain the following equations:

$$\left( \frac{\widehat{R}_y}{\mu} B_1 - B_2 k_{Tz} \right) e^{i(k_x x - \omega t)} = \frac{\widehat{R}_y}{\mu} u_y^{(m)} \tag{42}$$

$$\left( \frac{\widehat{R}_y}{\mu} B_3 + B_4 k_{Tz} \right) e^{i(k_x x - \omega t)} = \frac{\widehat{R}_y}{\mu} u_y^{(m)} \tag{43}$$

The equation of motion for the model described in Figure 16 is given by::

$$\widehat{m} \frac{d^2 u_y^{(m)}}{dt^2} = \widehat{R}_y \left( u_y^{(I)} - 2u_y^{(m)} + u_y^{(II)} \right) \tag{44}$$

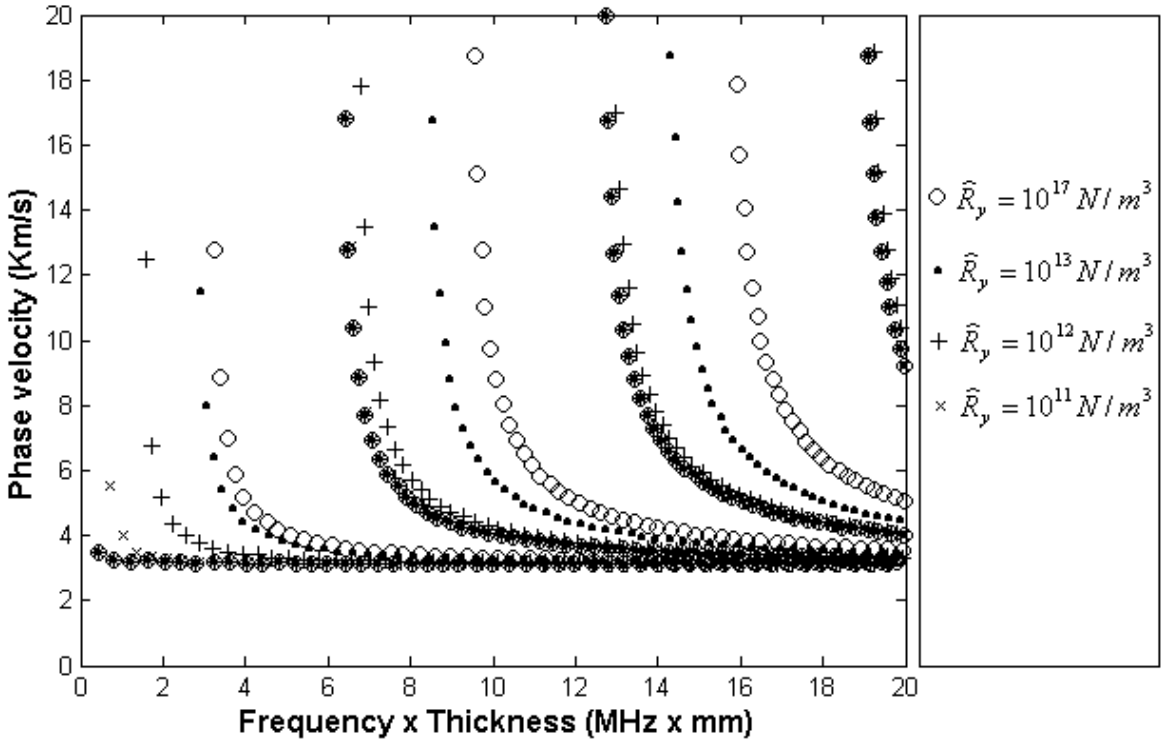


Figure 13: Dispersion curves.

where $\widehat{m} = \frac{m}{S}$ is the specific mass.
Using equations 31, 40 and 41, equation 44 may be rewritten in the form:

$$u_y^{(m)} = \frac{-\mu k_{Tz}}{\omega^2 \widehat{m}} \left(B_2 - B_4\right) e^{i(k_x x - \omega t)} \tag{45}$$

By applying Eq. 45 in Eqs. 42 and 43, we obtain the following equations:

$$\frac{\widehat{R}_y}{\mu} B_1 + \left(\frac{\widehat{R}_y k_{Tz}}{\omega^2 \widehat{m}} - k_{Tz}\right) B_2 - \frac{\widehat{R}_y k_{Tz}}{\omega^2 \widehat{m}} B_4 = 0 \tag{46}$$

$$\frac{\widehat{R}_y k_{Tz}}{\omega^2 \widehat{m}} B_2 + \frac{\widehat{R}_y}{\mu} B_3 + \left(k_{Tz} - \frac{\widehat{R}_y k_{Tz}}{\omega^2 \widehat{m}}\right) B_4 = 0 \tag{47}$$

Equations 34, 46 and 47 may be rewritten in matrix form:

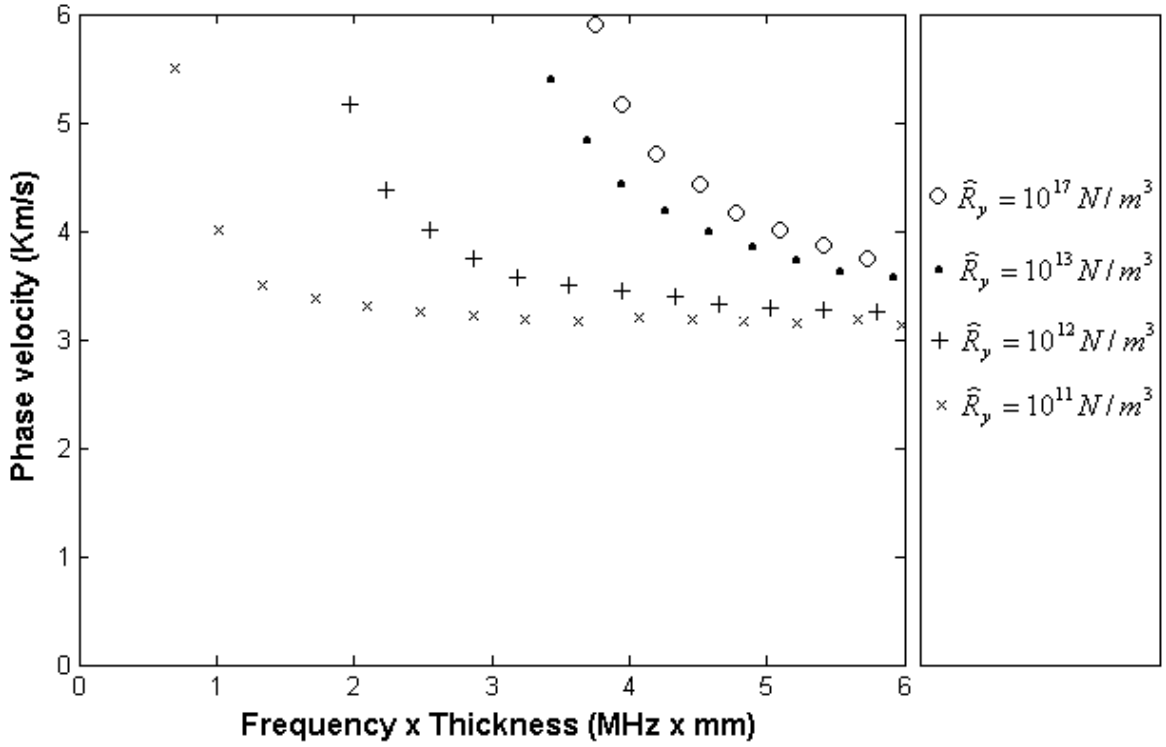


Figure 14: Dispersion curves for A0.

$$\begin{bmatrix} -\sin(k_{Tz}h_1) & \cos(k_{Tz}h_1) & 0 & 0 \\ 0 & 0 & \sin(k_{Tz}h_2) & \cos(k_{Tz}h_2) \\ \frac{\widehat{R}_y}{\mu} & \left(\frac{\widehat{R}_y k_{Tz}}{\omega^2 \widehat{m}} - k_{Tz}\right) & 0 & -\frac{\widehat{R}_y k_{Tz}}{\omega^2 \widehat{m}} \\ 0 & \frac{\widehat{R}_y k_{Tz}}{\omega^2 \widehat{m}} & \frac{\widehat{R}_y}{\mu} & \left(k_{Tz} - \frac{\widehat{R}_y k_{Tz}}{\omega^2 \widehat{m}}\right) \end{bmatrix} \begin{Bmatrix} B_1 \\ B_2 \\ B_3 \\ B_4 \end{Bmatrix} = 0 \qquad (48)$$

The solutions of the system of Eqs. 48 constitutes the dispersion curves. The solutions are given for vanishing determinate and they were calculated numerically using a routine implemented with the aid of the commercial code MATLAB$^{TM}$.

The dispersion curves of SH waves were obtained for different specific mass of the adhesive layer, while keeping the stiffness constant $\widehat{R}_y = 10^{17} N/m^3$. Figure 17 shows the influence of the specific mass on the dispersion curves of SH waves. This figure shows the dispersion curves of SH waves for $\widehat{m} = 0$; $\widehat{m} = 2Kg/m^2$; $\widehat{m} = 20Kg/m^2$ and $\widehat{m} = 200Kg/m^2$.

Note in Figure 17 that a small difference is detected in the dispersion curves for $\widehat{m} = 2Kg/m^2$ with respect to the dispersion curves for $\widehat{m} = 0$. For $\widehat{m} < 2Kg/m^2$ the dispersion curves are practically the same as the curves for $\widehat{m} = 0$. Taking into account that one of the most important

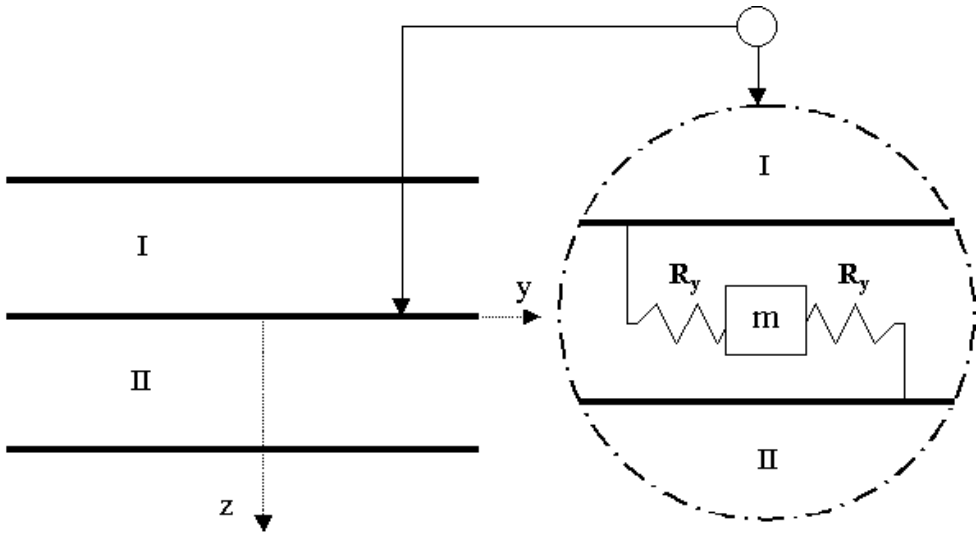


Figure 15: Model of the adhesive layer with distributed springs and masses.

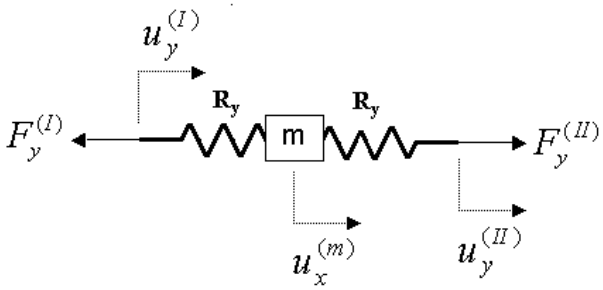


Figure 16: Forces and displacements on the springs.

characteristics of the adhesive bonds is the low weight, from the results shown in Figure 17 we concluded that the adhesive mass has little influence on the dispersion curves of SH waves for practical applications.

## 6 Conclusions

The quasi-static approximation was used to model the adhesive layer of two aluminium bonded plates to simulate the propagation of Lamb waves and SH waves. The dispersion curves of Lamb waves and SH waves were determined for different conditions of the adhesive layer by changing the stiffness constants of the springs. Comparisons among the dispersion curves for the perfect adhesion and the dispersion curves for deficient conditions of the adhesive layer, shown that

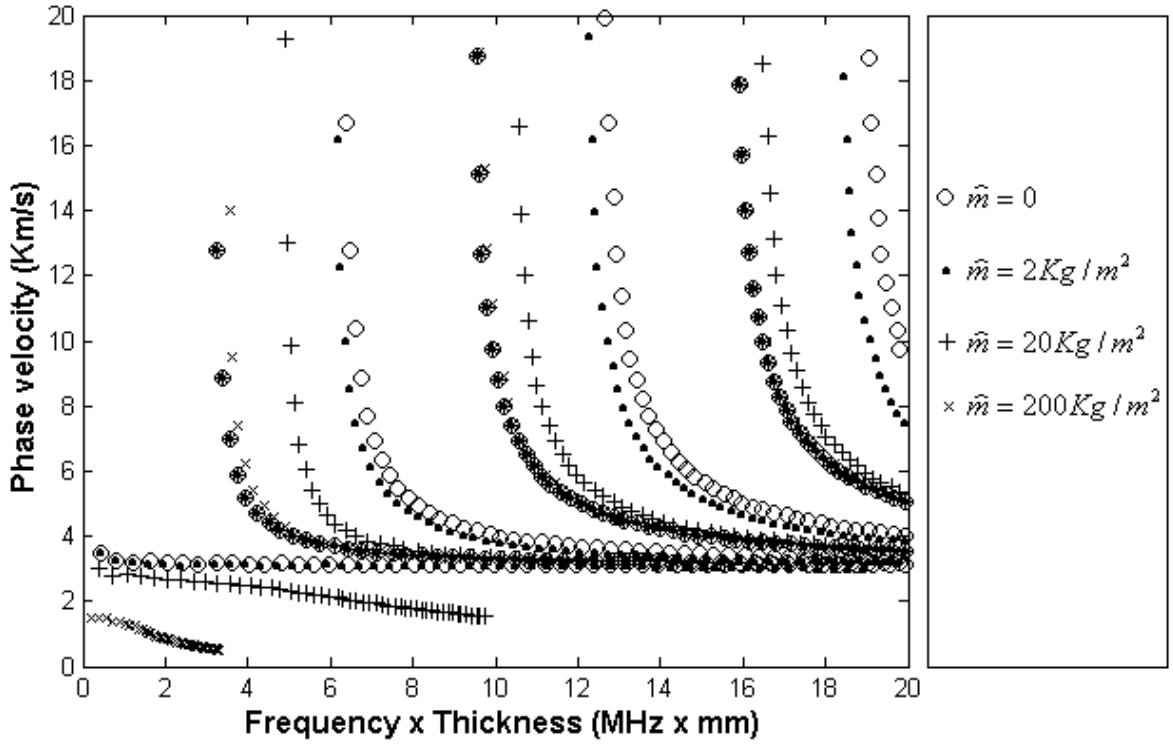


Figure 17: Dispersion curves.

the Lamb modes and the SH modes are sensitive to the alterations of the adhesive. We noted that the Lamb modes change accordingly with the stiffness constant modified. In the case of SH waves only the anti-symmetric modes change with the reduction of the stiffness constant. We also verified that in general, the phase velocity decreases when the stiffness constant of the springs are reduced.

The influence of the adhesive mass on the dispersion curves of SH waves was investigated. The results shown that for practical apllications the adhesive mass has little influence.

The theorical results presented in this work can be compared with acoustic test results in order to evaluate some interface parameters. This interface parameters are necessary in damage models used for the analysis of interface dedonding.

With the widespread use of the adhesive bonding and the lack of adequate tools of design and control, the results of this work shown that the inspection techniques based on guided waves have a great potential for the evaluation of bonded joints.

## References

[1] J.D. Achenbach. Wave propagation in elastic solids. North Holland, Amsterdam, 1975.

[2] G. Alfano and M. A. Crisfield. Finite element models for the delamination analysis of composite structures: mechanical and computational issues. Int. J. Num. Meth. Eng., 50:1701–1736.

[3] O. Allix and A. Corigliano. Modeling and simulation of crack propagation in mixed-modes interlaminar fracture specimens. Int. J. Fracture, 77:111–140, 1996.

[4] O. Allix, D. Leveque, and L. Perret. Identification and forecast of delamination in composite laminates by an interlaminar interface model. Composite Science and Technology, 185:671–678, 1998.

[5] J. M. Baik and R. B. Thompson. Ultrasonic scattering from imperfect interfaces: a quasi static model. J. Nondestructive Evaluation, 4:177–196, 1984.

[6] L. Champaney and N. Valoroso. A damage model for simulating decohesion in adhesively bonded assemblies. In ECCOMAS 2004, editor, Proc. European Congress on Computational Methods in Applied Sciences and Engineering, pages 24–28, Jyvaskyla, Finland, 2004.

[7] K. F. Graff. Wave motion in elastic solids. Dover Publications, 1991.

[8] C. C. H. Guyott and P. Cawley. The ultrasonic vibration characteristics of adhesive joints. J. Acoust. Soc. Am, 83(2):632–640, 1988.

[9] K. Heller, L.J. Jacobs, and J. Qu. Characterization of adhesive bond properties using Lamb waves, volume 33. NDT&E, 2000.

[10] M. Hirao and H. Ogi. An SH-wave EMTA technique for gas pipeline inspection, volume 32. NDT&E International, 1999.

[11] J. P. Jones and J. S. Whittier. Waves at flexibly bonded interface. J Appl. Mech, pages 905–908, 1967.

[12] A. Jungman, P. Guy, and G. Quentin. Characterization of glued bonds using ultrasonic reflected beam. Review of Progress in Quantitative Nondestructive Evaluation, 10B:1319–1327, 1991.

[13] T. Kundu and K. Maslov. Material interface inspection by lamb waves. Int. J. Solids Strucutures, 34:3885–3901, 1997.

[14] A. I. Lavrentyev and S. I. Rokhlin. Ultrasonic spectroscopy of imperfect contact interfaces between a layer and two solids. J. Acoust. Soc. Am, 103(2):657–664, 1998.

[15] B. Lombard and J. Piraux. How to incorporate the spring-mass conditions in finite-difference schemes. SIAM J. Scient. Comput., 24(4):1379–1407, 2003.

[16] M. J. S. Lowe and P. Cawley. The applicability of plate wave techniques for the inspection of adhesive and diffusion bonded joints. Journal of Nondestructive Evaluation, 13(4):185–200, 1994.

[17] K. Maslov and T. Kundu. Selection of lamb modes for detecting internal defects in composite laminates. Ultrasonics, 35:141–150, 1997.

[18] Y. Mi, M. A. Crisfield, G. A. O. Davies, and H.-B. Hellweg. Progressive delamination using interface elements. J. Composite Materials, 32(14):1246–1272, 1998.

[19] R. S. C. Monkhouse, P. W. Wilcox, M. J. S. Lowe, R. P. Dalton, and P. Cawley. The rapid monitoring of structures using interdigital lamb wave transducers. In 4th ESSM and 2nd MIMR conference, pages 397–404. Harrogate, 1998.

[20] V. Mustafa, A. Chahbaz, D. R. Hay, M. Brassard, and S. Dubois. Imaging of disbond in adhesive joints with lamb waves. NDTnet, 1997.

[21] P. B. Nagy and L. Adler. Nondestructive evaluation of adhesive joints by guided waves. Journal of Applied Physics, 66(10):4658–4663, 1989.

[22] C. Pecorari and P. A. Kelly. The quasistatic approximation for a cracked interface between a layer and a substrate. J. Acoust. Soc. Am, 107(5):2454–2461, 2000.

[23] A. Pilarski and J. L. Rose. A transverse wave ultrasonic oblique-incidence technique for interface weakness detection in adhesive bonds. J. Apll. Phys, 63:300–307, 1988.

[24] S. I. Rohklin and Y. J. Wang. Analysis of boundary conditions for elastic wave interaction with an interface between two solids. J. Acoust. Soc. Am., 89(1):503–515, 1991.

[25] S. I. Rokhlin. Lamb wave interaction with lap-shear adhesive joints: Theory and experiment. J. Acoust. Soc. Am., 89(2):2758–2765, 1991.

[26] R. Seifried, L. J. Jacobs, and J. M. Qu. Propagation of guided waves in adhesive bonded components. NDT&E International, 35(5):317–328, 2002.

[27] L. Singher, Y. Segal, E. Segal, and J. Shamir. Considerations in bond strength evaluation by ultrasonic guided waves. J. Acoust. Soc. Am., 96(4):2497–2505, 1994.

[28] V. Vlasie, S. de Barros, M. Rousseau, L. Champaney, H. Duflo, and B. Morvan. Mechanical and acoustical study of a structural bond : comparison theory/numerical simulations/experiment. 2004.

[29] V. Vlasie and M. Rousseau. Acoustical validation of the rheological models for a structural bond. Wave Motion, 37:33–349, 2003.

[30] P. C. Xu and S. K. Datta. Guided waves in a bonded plate: A parametric study. J. Appl. Phys., 67(11):6779–6786, 1990.

[31] C. H. Yew and X. W. Weng. Using ultrasonic sh-waves to estimate the quality of adhesive bonds - a preliminary-study. J. Acoust. Soc. Am., 77(5):1813–1823, 1985.